Jacob Herrmann
Roy J. Carver Department of Biomedical Engineering, University of Iowa, Iowa City, IA 52242

Michaela Kollisch-Singule
Department of Surgery, SUNY Upstate Medical University, Syracuse, NY 13210

Joshua Satalin
Department of Surgery, SUNY Upstate Medical University, Syracuse, NY 13210

Gary F. Nieman
Department of Surgery, SUNY Upstate Medical University, Syracuse, NY 13210

David W. Kaczka[1]
Roy J. Carver Department of Biomedical Engineering, University of Iowa, Iowa City, IA 52242;
Department of Anesthesia, University of Iowa, Iowa City, IA 52242;
Department of Radiology, University of Iowa, Iowa City, IA 52242
e-mail: david-kaczka@uiowa.edu

Assessment of Heterogeneity in Lung Structure and Function During Mechanical Ventilation: A Review of Methodologies

The mammalian lung is characterized by heterogeneity in both its structure and function, by incorporating an asymmetric branching airway tree optimized for maintenance of efficient ventilation, perfusion, and gas exchange. Despite potential benefits of naturally occurring heterogeneity in the lungs, there may also be detrimental effects arising from pathologic processes, which may result in deficiencies in gas transport and exchange. Regardless of etiology, pathologic heterogeneity results in the maldistribution of regional ventilation and perfusion, impairments in gas exchange, and increased work of breathing. In extreme situations, heterogeneity may result in respiratory failure, necessitating support with a mechanical ventilator. This review will present a summary of measurement techniques for assessing and quantifying heterogeneity in respiratory system structure and function during mechanical ventilation. These methods have been grouped according to four broad categories: (1) inverse modeling of heterogeneous mechanical function; (2) capnography and washout techniques to measure heterogeneity of gas transport; (3) measurements of heterogeneous deformation on the surface of the lung; and finally (4) imaging techniques used to observe spatially-distributed ventilation or regional deformation. Each technique varies with regard to spatial and temporal resolution, degrees of invasiveness, risks posed to patients, as well as suitability for clinical implementation. Nonetheless, each technique provides a unique perspective on the manifestations and consequences of mechanical heterogeneity in the diseased lung.
[DOI: 10.1115/1.4054386]

Introduction

By its very nature, the mammalian lung is characterized by heterogeneity in its structure, by incorporating an asymmetric, fractal-like branching airway and vascular trees optimized through evolution for maintenance of efficient ventilation, perfusion, and gas exchange within irregularly shaped boundaries [1]. The branching structure of airways also contributes to mixing and homogenization of regional gas concentrations, due to asymmetric variations in velocity profiles during inspiration and expiration, as well as repetitive division and recombination of gas flows originating from mechanically disparate lung regions. The structural composition and intrinsic mechanical properties of airway segments are also highly variable along the pathways between the trachea and alveolar spaces [2,3]. Structural heterogeneity and complexity are thus inherent characteristics of respiratory function [4], and may even serve a protective role in maintaining stability against perturbations [5,6], including abnormal conditions influencing morphogenesis and development [7]. Despite the potential beneficial effects of naturally occurring structural heterogeneity in the lungs, there may also be detrimental effects arising from pathologic processes, which may result in functional deficiencies in gas transport and exchange [8]. For example, progressive destruction of the parenchyma in emphysema, regional ventilation defects due to asthmatic bronchoconstriction, or alterations in parenchymal compliance in the acute respiratory distress syndrome (ARDS) can all occur in a heterogeneous pattern throughout the lung [9]. Regardless of etiology, such heterogeneity results in the maldistribution of regional ventilation and perfusion, impairments in gas exchange, and increased work of breathing. In extreme situations, pathologic heterogeneity may result in fulminant respiratory failure and require additional support with a mechanical ventilator. However, the presence of mechanical heterogeneity during positive pressure ventilation may also lead to regional overdistension (*volutrauma*) and/or repetitive recruitment and collapse (*atelectrauma*). The injuries associated with cyclic overdistension and recruitment are collectively termed ventilator-induced lung injury (VILI) [10]. Patients with heterogeneous lungs are particularly at risk for VILI, due to the increased prevalence of regional asymmetries in ventilation [11,12]. For example, atelectasis in one lung region may lead to overdistension in other lung regions [13]. Volutrauma and parenchymal rupture induced by regional overdistension may also result in local inflammation and edema, redistributing ventilation elsewhere and allowing for the development of injury in other regions [14]. Atelectatic regions which are repetitively recruited and collapsed during ventilation are subjected to injurious shear stresses, causing additional inflammation and cell death [15]. The parenchyma between collapsed (or edematous) alveoli and normal alveoli may sustain VILI by both atelectrauma and volutrauma, through a permeability-originated obstruction response that is self-perpetuating [15]. Regional lung injury may also result in the release of inflammatory mediators into the pulmonary and systemic circulation (*biotrauma*), potentially contributing to worsening respiratory failure and multiple organ failure [16]. Thus, VILI may become a spiraling process of progressively worsening lung

[1]Corresponding author.
Contributed by the Applied Mechanics Division Technical Committee on Dynamics & Control of Structures & Systems (AMD-DCSS) of ASME for publication in the Journal of Engineering and Science in Medical Diagnostics and Therapy. Manuscript received December 23, 2021; final manuscript received April 13, 2022; published online May 11, 2022. Editor: Ahmed Al-Jumaily.

injury (Fig. 1), wherein the amount of normally functioning lung diminishes over time as the amount of nonfunctioning injured lung rises, due to the increasing mechanical burden imposed by heterogeneously distributed ventilation [17].

Strategies for providing safe mechanical ventilation attempt to minimize the risk of VILI by using a combination of appropriate end-expiratory pressures to maintain lung recruitment, and small tidal volumes (or driving pressures) to avoid overdistension [18,19]. Such modalities are referred to as "lung-protective" ventilation, to emphasize the strategic goal of reducing the potential for further injury caused by volutrauma and atelectrauma. For example, standard clinical treatment of ARDS involves the use of low tidal volumes (i.e., $\sim$6 mL kg^{-1}), and a protocolized, stepwise decision sequence for modifying positive end-expiratory pressure (PEEP) and the fraction of inspired oxygen concentration (F_IO_2) based on the severity of hypoxemia [18]. Alternative protective ventilation strategies may also be considered, including oscillatory ventilation [20], biologically variable ventilation [21], or airway pressure release ventilation [22]. Several additional techniques have also been suggested to improve outcomes in patients with ARDS, including prone positioning [23], recruitment maneuvers [24], esophageal manometry [25], and chest wall strapping [26,27]. While the clinical evidence for the efficacy of these alternative modalities is very sparse [20], there is some evidence-based on computational modeling that these strategies may reduce the mechanical potential for VILI [28–31].

Understanding both natural and pathological heterogeneity in the lungs is thus essential for managing mechanical ventilation, and for determining the best ventilatory strategies for individual patients and specific diseases. Experimental methods for assessing regional lung distension and gas exchange in vivo are often limited in resolution. As a result, many experimental techniques require assumptions to infer global lung heterogeneity from either indirect measurement (e.g., alveolar pressure as a surrogate for alveolar distension) or partial observation (e.g., measurements made only near the lung surface). Despite limitations associated with performing and interpreting these measurements, accurate quantification of lung heterogeneity is valuable for diagnostic purposes, validation of computational models, and advancement of medical knowledge.

This review will present a summary of measurement techniques for assessing and quantifying heterogeneity in respiratory system structure and function during mechanical ventilation. These methods have been grouped according to four broad categories (Fig. 2): (1) inverse modeling of heterogeneous mechanical function; (2) capnography and washout techniques to measure heterogeneity of gas transport; (3) measurements of heterogeneous deformation on the surface of the lung; and finally (4) imaging techniques used to observe spatially-distributed ventilation or regional deformation. These measurement techniques provide unique, yet limited, perspectives on the manifestations and consequences of mechanical heterogeneity in the lung. As expected, each technique varies with regard to spatial and temporal resolution, degree of invasiveness, and risk posed to patients, as well as suitability for clinical implementation.

Inverse Modeling of Respiratory Mechanics

Heterogeneous processes in the lung are difficult to observe directly. Computational methods can be used to infer structural heterogeneity *via* inverse modeling of flows and pressures measured at the airway opening. This approach, known as *system identification*, abstracts the underlying mechanical complexity of the respiratory system into a minimal set of parameters to define a mathematical model. Inverse modeling of the respiratory system is usually performed by first recording transient waveforms of flow $\dot{V}(t)$ and pressure $P(t)$ at the airway opening [32]. The respiratory system is treated as a "black box" or unknown system, which may be identified by fitting several candidate mathematical models to sampled pressure and flow waveforms (e.g., using linear or nonlinear regression), and choosing the best prediction based on quantitative statistical comparison and/or qualitative interpretive judgment [32].

The simplest model used to characterize the lungs comprises a resistive element, primarily describing pressure losses due to flow through airways, in series with an elastic element, primarily describing pressure losses due to distension of compliant parenchymal tissues and/or chest wall (Fig. 3(*a*)). Assuming that resistive pressure fluctuations are linear with respect to flow with slope R, and elastic pressure fluctuations are linear with respect to changes in volume with slope E, the resulting relationship between pressure and flow becomes

$$P = R\dot{V} + EV + P_0 \tag{1}$$

where $\dot{V}$ and V are the observed flow and volume, respectively, into the lung. The pressure variable P may refer to the

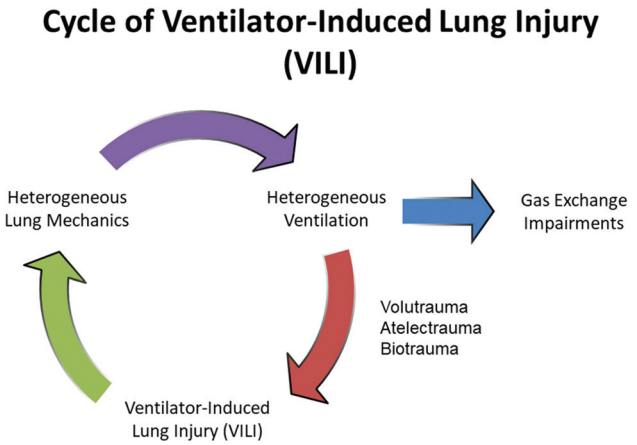

Fig. 1 The cycle of ventilator-induced lung injury (VILI). The presence of mechanical heterogeneity within the lung parenchyma results in the maldistribution of inspired volume and in impairments in gas exchange, due to the mismatching of regional ventilation and perfusion, as well as heterogenous CO_2 elimination. Regionally heterogeneous ventilation also may result in VILI, through the processes of volutrauma, atelectrauma, and biotrauma. VILI will then worsen existing lung mechanical heterogeneity.

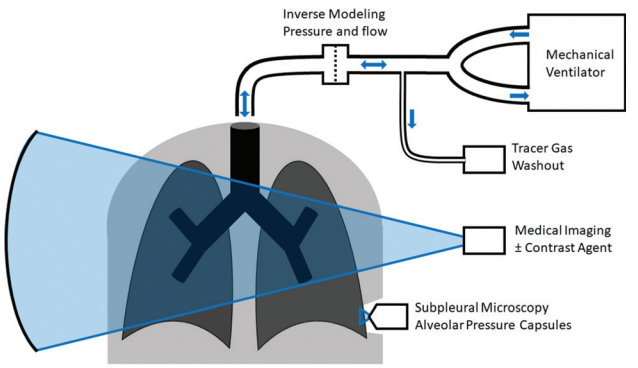

Fig. 2 Overview of various approaches used to assess heterogeneity during ventilation. Measurements of pressure, flow, and tracer gas concentrations at the airway opening allow assessment of lung function in terms of respiratory mechanics and gas exchange, but require careful inverse modeling approaches to indirectly infer heterogeneity based on time-varying measurements. Medical imaging modalities allow direct assessment of spatial heterogeneity in distributed ventilation via structural deformations across multiple images or contrast-enhanced imaging. Invasive measurements allow direct assessment of subpleural alveolar mechanics and deformations.

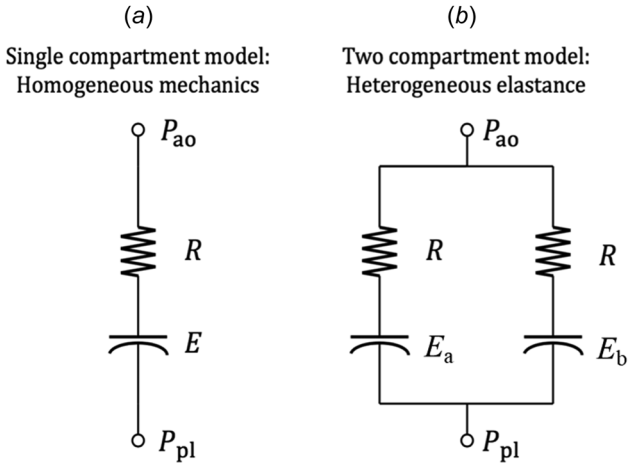

Fig. 3 Inverse models of respiratory mechanics, including pressure losses over resistive (*R*) and elastic (*E*) elements between the airway opening (P_{ao}) and the pleural space (P_{pl}): (*a*) single compartment model representing homogeneous airway resistance and tissue stiffness and (*b*) two-compartment model representing homogeneous airway resistance and a bimodal distribution of tissue stiffness

transpulmonary pressure across the lungs alone, the *intrapleural pressure* across the chest wall, or *transrespiratory pressure* across the lungs and chest wall together (i.e., if positive pressure variations are applied to the airway opening, as may occur during assisted mechanical ventilation). The P_0 is the corresponding distending pressure when flow at the airway opening is zero, and when the subject's lung volume is at a reference value at end-expiration. The mathematical model of Eq. (1) assumes a mechanically homogeneous lung by a single compartment, yet aptly predicts pressures and flows in healthy lungs during normal breathing [32]. Abnormal breathing and/or respiratory pathology often produce more complicated or nonlinear mechanical function [33–35], which can be described by increasing the complexity of Eq. (1).

Nonlinear elements describe pressure-flow or pressure–volume relationships that cannot be represented by a simple linear slope. Transient changes in lung structure, and the resulting changes in mechanical function, reflect heterogeneous processes that can be described by the predictive power of nonlinear elements. For example, Kano et al. identified a volume-dependent elastance to characterize intratidal variations in elastance caused by intratidal recruitment or overdistension [33]

$$P = R\dot{V} + (E_1 + E_2V)V + P_0 \tag{2}$$

The effective elastance of the lung at any given level of inflation is represented by two parameters: a linear component E_1 and a volume-dependent component E_2V. After model regression, the sign of E_2 and its magnitude relative to E_1 convey useful information about the presence and amount of global lung recruitment or overdistension. The relative amount of volume-dependent elastance can be described by the $\%E_2$ index

$$\%E_2 = \frac{E_2V}{E_1 + E_2V} \tag{3}$$

Large negative values of $\%E_2$ indicate decreasing lung elastance during inflation and suggest substantial recruitment of the lung. However, large positive values of $\%E_2$ indicate increasing lung elastance during inflation and may suggest strain-stiffening or overdistension of the parenchyma [36]. Thus, a heterogeneous distribution of recruitment or overdistension may be inferred from a nonlinear elastance model. However, $\%E_2$ may not always be a reliable discriminator of recruitment and overdistension, at least as measured with computed tomographic (CT) imaging in severely injured lungs [36]. The occurrence of both recruitment and overdistension simultaneously in different lung regions may produce counterbalancing variations in total lung elastance measured at the airway opening. Thus $\%E_2$ is only indicative of volume-dependence in total lung elastance and may be used to infer heterogeneous lung recruitment or overdistension only when the occurrence of these two processes is mutually exclusive.

Increased model complexity can also be achieved using an alternative arrangement of multiple resistive and elastic elements representing structural heterogeneity [9]. For example, a heterogeneous distribution of tissue elastance in patients might be described by a two-compartment heterogeneous elastance model, as shown in Fig. 3(*b*). The equation of motion for this system is given by [32]

$$2R\dot{P} + (E_a + E_b)P = R^2\ddot{V} + (E_a + E_b)R\dot{V} + E_aE_bV + P_0 \tag{4}$$

Note that the model complexity of Eq. (4) has increased greatly compared to Eq. (1). Despite the addition of only one new parameter (E_b), two new higher-order derivatives of pressure and flow are required. Due to increasing analytical and computational complexity associated with the regression of multicompartmental models in the time domain [37], frequency-domain analysis may at times be preferable. The transfer function relating pressure and flow in this system as a function of frequency (f) is described by its mechanical impedance Z

$$Z(f) = \left[\left(R + \frac{E_a}{j2\pi f}\right)^{-1} + \left(R + \frac{E_b}{j2\pi f}\right)^{-1}\right]^{-1} \tag{5}$$

where $j = \sqrt{-1}$. As a function of f, Eq. (5) yields a complex-valued spectrum, with real part describing energy dissipation (i.e., in-phase pressure and flow oscillations) and imaginary part describing energy storage (i.e., out-of-phase pressure and flow oscillations). Respiratory impedance Z can be measured in vivo at multiple values of f using various oscillometric techniques [38], such as the application of pseudo-random broadband flow and pressure excitations at the airway opening and estimation of the transfer function [39]. The patient's impedance spectrum may then be fit by the model-predicted impedance at the measured frequencies [39,40].

Otis et al. defined a model of lung heterogeneity identifying two conceptual compartments (i.e., not necessarily distinct anatomic structures) with different mechanical time constants [41]. Otis' findings suggested a mechanism by which lung regions with different resistive and elastic properties could not only receive different proportions of the volume delivered at the airway opening but could also receive their respective volume oscillations at different phases of the oscillatory cycle relative to each other [41]. Glapinski et al. described a metric for estimating mechanical heterogeneity based on fitting the Otis model to measured data and subsequently computing the ratio of mechanical time constants between the two compartments [42]. Other investigators have defined models of heterogeneously distributed mechanical properties, such as airway resistance and tissue elastance, characterized by predefined probability distributions [35,43–46]. When fit to mechanical impedance spectra of either anatomically-structured computational models [47] or animal models of heterogeneous lung injury [48], these heterogeneous models described the presence, severity, and distribution of the mechanical heterogeneity within the lungs.

While increasing complexity of a model may increase its predictive power, it is possible that any additional parameters may yield no meaningful contribution to its physiologic interpretation or relevance. Accordingly, excessive complexity inhibits the interpretive usefulness of a model, potentially obfuscating the strongest predictors of nonlinear mechanical function amidst an array of superfluous parameters. Often, the greatest amount of information is gleaned from *minimally complex* models. In other words, the

most useful model employs the fewest parameters required to achieve a reasonably accurate prediction of observed mechanical function.

Statistical comparisons such as the Akaike information criterion favor models that more closely describe the observations, yet disfavor models with greater numbers of parameters, quantitatively balancing predictive power against complexity [32,47,49]. Nonetheless, no statistical comparison is capable of determining the physical and physiologic relevance of a model regression—a qualitative judgment is also required. For example, negative elastance parameters violate physical assumptions of pressure–volume interaction in compliant compartments. Likewise, values of elastance too small or too large to realistically describe lung tissue compliance may be considered physiologically irrelevant. Both cases suggest that the model in question does not appropriately describe the mechanical structure of the respiratory system which generated the observed data. Although parameter regressions that yield nonphysical or nonphysiologic values may present quantitatively superior fits, their exclusion may be warranted based on qualitative judgment. Whenever possible, model selection should consider a priori information about the patient or subject.

Capnography and Washout Techniques

Volume capnography is the measurement of the carbon dioxide (CO_2) concentration (or partial pressure) at the airway opening during expiration, as transported by advective and diffusive mechanisms from the alveolar spaces *via* the conducting airways [50]. Figure 4 shows an example of CO_2 concentration as a function of exhaled gas volume. This concentration is expected to be minimal (i.e., near zero) during the initial expiratory phase, since the initial portion of expired gas originates within the larger conducting airways (i.e., dead space) at end-inspiration, where no respiratory gas exchange occurs. The final portion of expired gas originates with the alveolar spaces at end-inspiration, and thus contains higher concentrations of CO_2 and lower concentrations of oxygen than dead space gas. Between the initial and final expiratory phases, there is a transitionary phase during which expired gas comprises a mixture of both dead space and alveolar gases. The profile of CO_2 plotted against time or exhaled volume, especially during the transitionary and final phases, are sensitive indicators

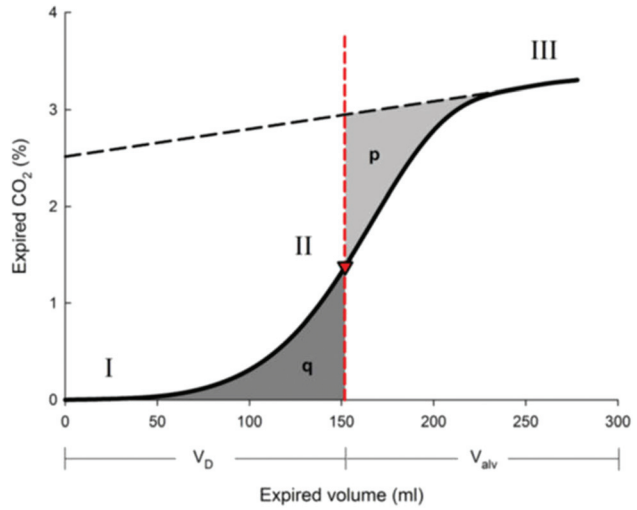

Fig. 4 Example volume capnograph for estimation of anatomic dead space. Percent of exhaled CO_2 is plotted against exhaled gas volume for a single breath. A line tangent to phase III (sloping upward dashed) and a vertical line through phase II (vertical dashed) are positioned such that areas p and q are equal. Volumes along the x-axis to the left and right of the vertical line are assumed to correspond to the dead space volume (V_D), and the effective alveolar volume (V_{alv}), respectively. Reproduced with permission from Ref. [132]. Copyright 2018.

of several anatomic and physiologic factors [51–54]: (1) asymmetry of the anatomic dead space, or the volume of the conducting airways, (2) physiologic dead space, or the volume of alveolar spaces with deficient gas exchange, and (3) heterogeneous distribution of inspired and expired volume. Volume capnography may be useful for determining the overall degree of ventilation-perfusion heterogeneity relative to normal exhaled CO_2 profiles [55]. However, the technique may be limited by the difficulty of discerning the relative contributions from each of the three aforementioned sources of heterogeneity in gas transport.

Alternatively, multiple-breath washout techniques use an inert and minimally soluble tracer gas (e.g., nitrogen), rather than CO_2, by first equilibrating the tracer gas throughout the lungs and then measuring its rate of elimination during tidal breathing (e.g., using 100% inspired oxygen) [56]. Unlike CO_2, the tracer is not replenished between breaths. Depending on the solubility of the tracer in the blood, its exhaled concentration will largely be independent of the distribution of perfusion. The number of breaths required to clear the lung of the tracer gas (or at least equilibrate alveolar and ambient concentrations), quantified by the lung clearance index, may provide a robust and sensitive indicator of ventilation heterogeneity [57,58]. Other indices obtained from the washout may quantify functional heterogeneities associated with convective and diffusive transport processes, and provide general anatomic information as gas transport shifts from conductive to acinar airways [59]. There are also empiric descriptions of the distributions of ventilation time constants for quantifying heterogeneity [60]. However, without the combined use of imaging techniques (as discussed below), multiple-breath washout does not provide spatial information about the regional distribution of gas transport.

The multiple inert gas elimination technique (MIGET) is a more powerful measurement technique, relying on gas transport heterogeneity to predict distributions of ventilation and perfusion. Here, a dissolved mixture of different inert gases (typically six or more) with unique blood-gas partition coefficients is intravenously infused, and the resulting steady-state retention and excretion rates of each gas are measured using gas chromatography on samples of arterial blood and mixed expired gas, respectively [61,62]. The retention and excretion rates for all gases can then be regressed by a computational model comprising lung compartments with distributed ventilation-to-perfusion ratios ($\dot{V}/\dot{Q}$), yielding distributions of gas flow and blood perfusion apportioned into each $\dot{V}/\dot{Q}$ compartment [63,64]. The predicted $\dot{V}/\dot{Q}$ distributions provide insight into the size and severity of over-ventilated, under-ventilated, and shunted compartments. However, such compartments are purely conceptual, and consequently do not represent anatomic structures.

Lung Surface Measurements

Measurements of distributed lung deformation and pressure can be made directly on the surface of exposed or excised lungs such as in stroboscopic photography and videomicroscopy. Typically, these measurements require surgical sternotomy, thoracotomy, and/or total lung excision to expose the lung surface, which removes the influence of the chest wall on the mechanics of ventilation. Although lung surface measurements are not viable for clinical use in patients, information learned from research studies which directly visualize the response of alveoli to changes in mechanical ventilation settings has offered a unique insight into locoregional heterogeneity and has informed general mechanical ventilation practice guidelines [65]. Stroboscopic photography measures surface deformations during periodic motion, with synchronization between camera and strobe light to capture a series of still images spaced evenly throughout the ventilatory cycle. Using this technique, Lehr et al. [66] found increased heterogeneity in the distributions of both magnitude and phase of lung surface deformations during high-frequency oscillatory ventilation, suggesting that ventilation throughout the lung may be nonuniform and asynchronous at high frequencies compared to

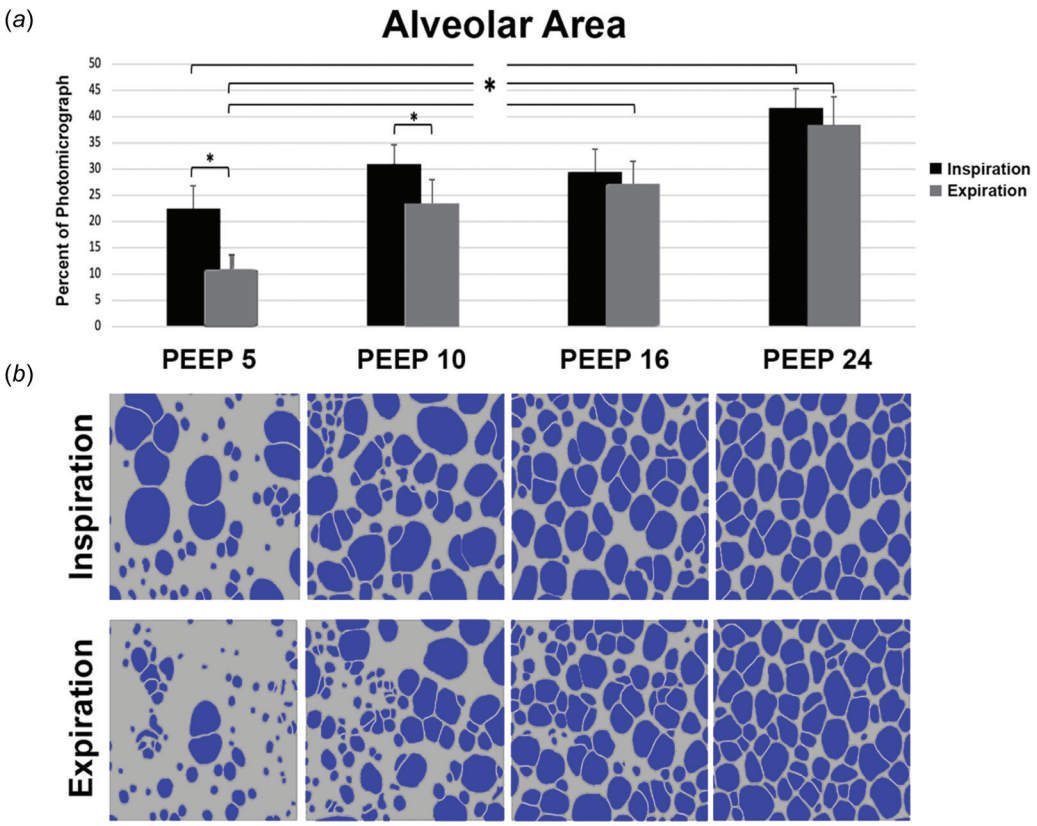

Fig. 5 In Vivo photomicrographs of subpleural alveoli in a Tween-injured lung at inspiration and expiration with individual alveoli identified, outlined, and colored with subsequent quantification of area. The area of inflated alveoli is reported as a percentage of the total photomicrograph (*a*). Alveoli were analyzed at varying PEEP levels: 5, 10, 16, and 24 cm H_2O. Alveoli are colored in blue and nonalveolar tissue in gray (*b*). Data are shown as the mean with error bars indicate standard error of the mean. *$p < 0.05$ between groups and between inspiration and expiration within group. Adapted from Ref. [65].

conventional breathing frequencies. Stroboscopic photography is especially advantageous for capturing lung motion at high frequencies of oscillation without blur artifact when cameras with high frame rates are not accessible. Other specialized image acquisition and processing techniques may be used to assess lung surface deformations during ventilation with conventional frequencies. For example, digital image correlation may be performed with multiple cameras acquiring images from different perspectives, allowing reconstruction of a three-dimensional model of the lung surface and estimation of regional surface strains dynamically during ventilation [67].

Videomicroscopy is a video capture technique utilizing high-powered objective lenses, whereby it is possible to generate individual alveolar area/airway pressure curves to analyze the dynamic changes occurring in alveoli (Fig. 5) [65,68]. Namati et al. [69] developed a similar optical confocal process to measure alveolar dynamics during quasi-static inflation and deflation maneuvers and showed that recruited alveoli become smaller and more numerous after inflation, suggesting that normal, physiologic tidal volume change is modified by alveolar recruitment rather than expansion. In a separate videomicroscopy study [70], recruited alveoli were found to have a normal size distribution without demonstration of large, overdistended alveoli. However, surfactant de-activation led to a heterogeneous alveolar distribution with two general subsets: a large population of small, collapsed alveoli, and a smaller population of large, overdistended alveoli. The application of higher mean airway pressures partially attenuated the effects of surfactant de-activation by revealing a more homogeneous set of alveoli, but never achieved a normal distribution after deflation [70]. These findings were supported by Mertens et al. [71], who showed that loss of compliance in injured alveolar clusters resulted in the redistribution of inspired tidal volumes to more compliant (but larger) alveoli, potentially promoting alveolar distension and overall spatial heterogeneity.

In either case, the primary limitations of lung surface analyses are: (1) restricted imaging of only the outer surface of the lung, which may not accurately reflect deformations throughout the majority of parenchyma where there is increased alveolar interdependence; (2) the loss of information incurred during the reduction of spatial dimensions when projecting three-dimensional motion onto two dimensions; (3) stabilization of the moving lung during imaging, introducing further artifact [70]; (4) absence of the lung and chest wall interactions secondary to an open chest; and (5) inability to evaluate the conducting airways, which also demonstrate heterogeneous motion [72].

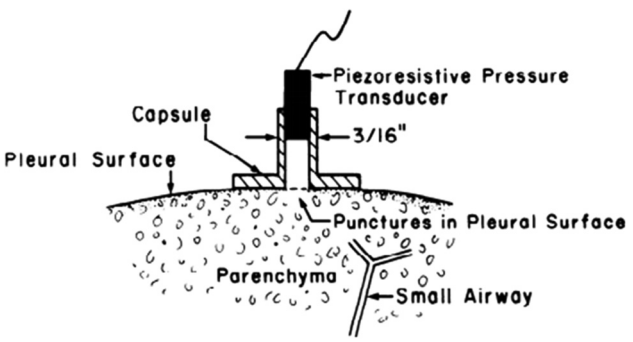

Fig. 6 Example of the alveolar capsule system used by Fredberg et al. to measure alveolar pressure. Reproduced with permission from Ref. [73]. Copyright 1984 by APS.

Alternatively, alveolar pressures near the lung surface may be directly measured using alveolar capsules. Each capsule is bonded and hermetically sealed to a small region of the lung surface, after which a puncture of the pleural surface through the center of the capsule exposes a pressure transducer directly to pressure variations in the alveolar spaces [73], and quantifies local magnitudes and phases of surface alveolar pressures during ventilation (Fig. 6). Alveolar capsules have been used in a number of studies investigating mechanical heterogeneity of the lungs during oscillometric impedance measurements [74,75], bronchoconstriction [76,77], and lung recruitment [78]. The technique provides a direct measurement of alveolar pressure at the lung surface. However, such direct measurements may not necessarily be representative of the actual distribution of alveolar pressures throughout the entire lung, and thus cannot be used to infer the heterogeneity of ventilation distribution.

Lung Imaging

Medical imaging technology produces spatially-oriented distributions of a measured property, depending on technique. The interpretation of any imaging data depends on the image quality, which in turn depends on several factors including spatial resolution, signal-to-noise ratio, sharpness, and absence of artifacts. For example, X-ray imaging passes high-energy photons through a subject, to construct a spatially-oriented distribution of absorption or scatter. A plain chest radiograph may be the most readily available X-ray modality for lung imaging at the bedside, although as a two-dimensional projection, it may not convey sufficient spatial information of heterogeneous pathologic processes for diagnosis or monitoring treatment [79].

Three-dimensional images describing lung structure and anatomy may be obtained using CT imaging. The high dynamic range and high contrast of radiodensity values facilitates distinction of air, tissue, and bone. The linearity of the radiodensity scale facilitates the calculation of the relative amounts of air and tissue within each lung voxel, yielding spatial distributions of lung aeration [80]. Submillimeter resolution in CT images facilitates the segmentation of lung external boundaries, airways, blood vessels, and fissures [81–84]. Thus, heterogeneity in the lung can be observed directly using CT imaging, which reveals characteristic alterations in the structure and/or aeration for pathologies such as metastatic cancer, emphysema, pulmonary fibrosis, or pulmonary edema. Moreover, heterogeneity of the measured property can be directly assessed by statistical methods applied to the voxels within the lung [80,85].

Computed tomographic image acquisition occurs over several seconds, during which the subject usually remains motionless to minimize blurring in the resulting image. This restriction limits the use of CT for observing dynamic processes such as changes in lung structure during inspiratory and expiratory phases of breathing. CT methods for approximating dynamic alterations in lung structure use either quasi-static approaches [48,86], or respiratory-gated acquisition [87,88] both of which require scanning the subject multiple times. The resulting four-dimensional images can be used to visually track spatial changes in regional aeration, lung recruitment, and anatomical landmarks (Fig. 7). Volumetric deformations may be quantifiably assessed using image registration techniques that compute a spatial transformation between images representing different inflation levels or different breath phases [89,90]. Thus heterogeneity in the distribution of flow throughout the lung can be measured using four-dimensional reconstruction

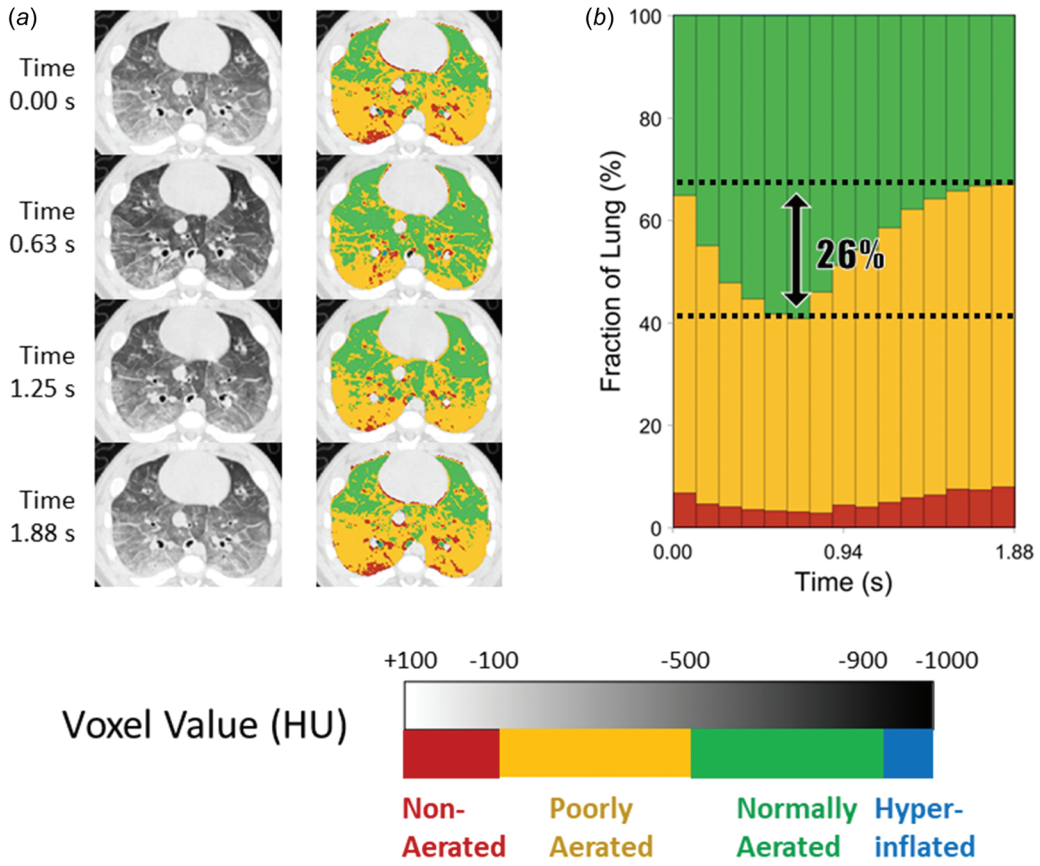

Fig. 7 Changes in regional aeration during porcine oleic acid lung injury obtained using dynamic CT reconstruction [91]. Ranges of CT Hounsfield density correspond to levels of lung aeration: (*a*) transverse sections of the CT images are shown at four time points during a single pressure-controlled breath. (*b*) time course of aeration levels during the breath. Note that 26% of the imaged lung cyclically alters between normally and poorly aerated levels during the breath. Data modified from Ref. [92].

[91,92], in combination with deformable image registration [93]. Further insight into heterogeneity of tissue mechanical properties and regional response to changes transpulmonary pressure may be gained through the interpretation of image-based deformation models with specific material assumptions (e.g., poroelastic models of lung parenchyma [94,95].

Magnetic resonance imaging (MRI) historically has had limited applications in imaging respiratory motion due to prohibitively long acquisition durations, as well as low proton density in lung tissues. Multiple breath-holds are required for some MRI sequences, producing images in which finer anatomic structures are not apparent in part due to blurring caused by breath-to-breath variability [96–98]. Two-dimensional acquisition supports much greater acquisition rates compared to full three-dimensional imaging (e.g., of the order of 10 Hz [99,100]), yet produces only a single cross section of the thoracic cavity. Image registration techniques are not applicable to two-dimensional imaging because the computational methods cannot account for motion in the direction orthogonal to the acquired plane. Modern advancements in MRI technology and signal processing algorithms have substantially improved acquisition capabilities. Recently developed sequences can provide two-dimensional image acquisition at rates up to 100 Hz [101]. Other advancements include the use of parallelized acquisition, compressed sensing, and sparse reconstruction to achieve 2–15-fold increases in sampling rate [102–104].

Differentiating between air and parenchymal tissues in MRI remains a challenge, despite the use of high-acquisition-rate techniques to mitigate motion artifact. Signal-to-noise ratio is inadequate because of the low overall proton density throughout the lung, and furthermore because of the large differences in magnetic susceptibility at the interfaces between air and parenchymal tissues [96–98]. Ultrashort echo time (UTE) sequences have been investigated as a means of resolving MRI signals from parenchymal tissues [105]. Other MRI methods directly measure the mechanical properties of the tissues, instead of deformation. For example, magnetic resonance elastography is used to estimate distributed shear stiffness in parenchymal tissues by applying shear waves at frequencies up to 200 Hz and measuring the resulting MRI signal phase variability caused by small-amplitude tissue displacement [106,107]. Other approaches involve selectively tagging lung parenchyma with a magnetization pattern, a technique known as spatial modulation of magnetization (SPAMM), and subsequently measuring deformations in the magnetized pattern during breathing [108], using a similar two-dimensional analysis applied to deformations in patterns marked on the surface of ventilated lungs [66]. MRI methods are incredibly varied and complicated, and may yet come to rival 4DCT methods in spatial and temporal resolution of lung structure, enabling quantitative assessment of distributed respiratory mechanics without harmful radiation exposure.

As a surrogate for flow heterogeneity or lung deformation heterogeneity, gas transport heterogeneity can be measured directly using several imaging modalities, most involving the combination of an anatomic map of the respiratory system overlaid with spatially distributed values of a tracer gas concentration. Such imaging modalities include dual-energy X-ray CT in combination with radiodense xenon or krypton tracer [109,110], positron emission tomography (PET) in combination with radioactive isotope nitrogen-13 tracer [111], single-photon emission computed tomography (SPECT) with a radioactive tracer gas such as krypton-81m or technetium-99m [112], and MRI in combination with hyperpolarized helium-3 or xenon-129 tracer [85]. Temporal variations in tracer gas concentration within a given lung region indicate the regional action of advective and diffusive transport phenomena [113]. SPECT imaging is used in both research and clinical settings to assess ventilation and/or perfusion, with a high correlation between regional ventilation heterogeneity and heterogeneity indices derived from multiple-breath washout [114,115]. Hyperpolarized gas MRI using xenon-129 is emerging as a powerful modality for functional imaging due to the ability to differentiate xenon signals originating from the airspaces, blood, and interstitial tissue [116,117], in addition to the ability to assess apparent diffusion coefficient via diffusion-weighted imaging [118]. Recent methods using both PET and CT imaging data, combined with computational modeling, can estimate regional gas exchange as distributions of oxygen uptake and CO_2 elimination [119].

Electrical impedance tomography (EIT) measures changes in the electrical impedance (equivalent to the inverse of conductance) of tissues using a series of electrodes placed on the surface of the subject, usually forming a ring around the heart and lungs in the transverse plane [120]. Air spaces inside the lung exhibit higher electrical impedance than the tissues containing water and electrolytes, thereby providing contrast in the electrical impedance image and a means of assessing spatially distributed aeration. EIT images are usually compared to a reference image at a baseline lung volume (e.g., functional residual capacity at end-expiration), such that the resulting "difference" image provides spatially distributed *changes* in aeration [121]. Difference EIT is useful clinically for detecting pneumothoraces, lung collapse, as well as intratidal recruitment and derecruitment [122]. EIT images can be acquired at extremely fast rates (i.e., of the order of milliseconds per frame). Fourier analysis of individual voxels in images acquired faster than 60 frames per second can resolve frequency content in voxel aeration up to 30 Hz, demonstrating utility for the assessment of heterogeneous ventilation distribution even during high-frequency ventilation [123]. Temporal fluctuations in EIT signal can be processed according to respiratory rate and heart rate to assess coarse intratidal ventilation and perfusion dynamics, with potential contrast enhancement *via* hypertonic saline [122]. The primary challenge of using EIT is the difficulty of solving the ill-posed inverse transformation, which converts electrical impedance measurements at the boundary of an object into spatial distributions of impedance (and hence aeration) within the object [124]. Solutions are nonunique, highly-sensitive to noise, and highly dependent on the specific geometry of the subject. Accordingly, current EIT approaches produce images representing feasible and stable solutions yet with an extremely low spatial resolution (i.e., of the order of centimeters in adult patients), despite temporal resolution of the order of milliseconds. Improved spatial resolution can be achieved to an extent by increasing the number of electrodes [125]. Another limitation of EIT is its reliance on a single ring of an electrode array, which results in only a two-dimensional cross section with large slice thickness. Recent investigations into three-dimensional approaches using electrodes arranged in multiple transverse rings [126–129] may provide improved localization of changes in aeration within each image slice. Nevertheless, detection of ventilation heterogeneity using EIT remains limited to large spatial scales despite the excellent temporal resolution.

The primary utility of any imaging modality for the quantitative assessment of heterogeneous gas transport, aeration, or mechanical properties in the lung is its ability to present spatial and anatomic information. Imaging modalities offer direct measurement of distributed properties throughout lung tissues in the context of local anatomic structure, whereas the previously discussed methodologies may only infer whole-lung heterogeneity based on measurements performed at the airway opening or pleural surface. Disadvantages of imaging methods include high cost and scarcity of contrast and tracer agents, exposure to ionizing radiation, and high computational costs associated with image reconstruction, storage, and processing [84,91]. Continuing advancements in detector technology and reconstruction algorithms offer improvements in image quality and spatial resolution, as well as reductions in radiation exposure. Additionally, advancements in computational hardware and machine learning algorithms may yield automated feature extractions with substantial reductions in computational overhead [130].

Implications for Mechanical Ventilation

The ultimate motivation for measuring mechanical heterogeneity in the lung is the prospect of improving patient care and

reducing the morbidity and mortality associated with respiratory failure and disease. Ventilator-induced lung injury (VILI) remains a major risk for patients receiving positive pressure mechanical ventilation, due to excessive parenchymal strain and repetitive atelectasis. VILI is progressively worsened by mechanical heterogeneity in lung tissues, which results in maldistribution of ventilation. Nonetheless, the spatial distributions of ventilation and tissue mechanical properties are difficult to measure or observe directly in critically ill patients.

Measurements made at the airway opening (including washout techniques and impedance measurements) may be sensitive to changes in the overall degree of heterogeneity in lung structure and/or function, yet provide an only indirect assessment of the distributed values, and thus nothing on supplementary spatial correspondence. Direct transduction of mechanical signals is possible only through highly invasive procedures that may comprise the integrity of the lung and/or disrupt its normal function (e.g., surgery to expose and/or penetrate the pleural surface), and is therefore unsuitable for many research applications. Accordingly, the best approaches for precise measurement of regional parenchymal strain within an intact respiratory system during tidal ventilation involve using quasi-static or respiratory-gated CT or MR imaging, in combination with image registration [48,85,93]. However, imaging techniques may lose practical clinical utility for in vivo heterogeneity assessment if the subject is ventilated at extremely fast rates, given that image quality is diminished by motion artifacts that cannot be compensated using current reconstruction approaches. Measurement of distributed flow and parenchymal strain throughout the lung during ventilation at high frequencies may currently not be achievable with most available CT methodologies, without substantial exposure to ionizing radiation [93].

Conclusions

Useful measurements of ventilation heterogeneity in healthy and diseased lungs provide direct quantification of distributed properties such as flow, pressure, and gas composition. However, improved spatial resolution of a measurement technique often comes at the cost of increased invasiveness and/or risk to the patient. Direct measurements of heterogeneous lung function or structure are difficult to obtain in critically ill patients, given the risks involved in measurement (e.g., patient transport, suspension of mechanical ventilation) which may offset the potential diagnostic or therapeutic benefit of the information obtained. Indirect measurement techniques that are clinically feasible in critically ill patients can provide useful information about inferred lung heterogeneity, especially when such results can be validated using direct high-resolution spatial and temporal measurements. Measurements of lung heterogeneity offer valuable diagnostic information on the pattern and extent of lung injury, and may provide decision support for the selection and management of alternative mechanical ventilation modalities that minimize the adverse impact of pathological heterogeneity in critically ill patients. Future directions for improving the clinical utility of lung heterogeneity assessment could involve training artificial intelligence models to predict lung heterogeneity indices derived from direct measurement techniques, using point of care data from indirect measurements more easily obtained at the bedside. Machine learning models for the detection of patterns representing underlying heterogeneity may even surpass rule-based approaches to inverse modeling and system identification [84,130,131], without the inherent restrictions of compartmentalized structures or regression equations.

Acknowledgment

This work was supported by the Office of the Assistant Secretary of Defense for Health Affairs, through the Peer Reviewed Medical Research Program under Award Nos. W81XWH-16-1-0434, W81XWH-20-1-0696, and W81XWH-21-1-0507. Opinions, interpretations, conclusions, and recommendations are those of the authors and are not necessarily endorsed by the Department of Defense. This study was also supported by the Department of Anesthesia at the University of Iowa Hospital and Clinics, as well as National Institutes of Health awards R41 HL140640, R01 HL142702, and T32 HL144461.

Funding Data

- Congressionally Directed Medical Research Programs (Funder ID: 10.13039/100000090).
- National Heart, Lung, and Blood Institute (Funder ID: 10.13039/100000050).

Conflict of Interest

JH and DWK are cofounders and shareholders of OscillaVent, Inc., and are co-inventors on U.S. and European patents involving multifrequency oscillatory ventilation. JH and DWK serve as consultants for ZOLL Medical Corporation. DWK is a consultant for Lungpacer Medical, Inc. MKS and GFN have received honoraria and/or travel reimbursement at event(s) sponsored by Dräger Medical Systems, Inc. as well as an unconditional educational grant, outside of this work. GFN and MKS have lectured for Intensive Care Online Network, Inc. (ICON).

References

[1] Suki, B., Bates, J. H. T., and Frey, U., 2011, "Complexity and Emergent Phenomena," Compr. Physiol., **1**(2), pp. 995–1029.
[2] Eskandari, M., Arvayo, A. L., and Levenston, M. E., 2018, "Mechanical Properties of the Airway Tree: Heterogeneous and Anisotropic Pseudoelastic and Viscoelastic Tissue Responses," J. Appl. Physiol. (1985), **125**(3), pp. 878–888.
[3] Eskandari, M., Nordgren, T. M., and O'Connell, G. D., 2019, "Mechanics of Pulmonary Airways: Linking Structure to Function Through Constitutive Modeling, Biochemistry, and Histology," Acta Biomater., **97**, pp. 513–523.
[4] Weibel, E. R., 2009, "What Makes a Good Lung?," Swiss Med. Wkly., **139**(27–28), pp. 375–386.
[5] Florens, M., Sapoval, B., and Filoche, M., 2011, "The Optimal Branching Asymmetry of a Bidirectional Distribution Tree," Comput. Phys. Commun., **182**(9), pp. 1932–1936.
[6] Leary, D., Winkler, T., Braune, A., and Maksym, G. N., 2014, "Effects of Airway Tree Asymmetry on the Emergence and Spatial Persistence of Ventilation Defects," J. Appl. Physiol., **117**(4), pp. 353–362.
[7] West, B. J., 1990, "Physiology in Fractal Dimensions: Error Tolerance," Ann. Biomed. Eng., **18**(2), pp. 135–149.
[8] Rutting, S., Chapman, D. G., Farah, C. S., and Thamrin, C., 2021, "Lung Heterogeneity as a Predictor for Disease Severity and Response to Therapy," Curr. Opin. Physiol., **22**, p. 100446.
[9] Kaczka, D. W., Lutchen, K. R., and Hantos, Z., 2011, "Emergent Behavior of Regional Heterogeneity in the Lung and Its Effects on Respiratory Impedance," J. Appl. Physiol., **110**(5), pp. 1473–1481.
[10] Slutsky, A. S., and Ranieri, V. M., 2013, "Ventilator-Induced Lung Injury," N. Engl. J. Med., **369**(22), pp. 2126–2136.
[11] Colletti, A. A., Amini, R., and Kaczka, D. W., 2011, "Simulating Ventilation Distribution in Heterogenous Lung Injury Using a Binary Tree Data Structure," Comput. Biol. Med., **41**(10), pp. 936–945.
[12] Amini, R., and Kaczka, D. W., 2013, "Impact of Ventilation Frequency and Parenchymal Stiffness on Flow and Pressure Distribution in a Canine Lung Model," Ann. Biomed. Eng., **41**(12), pp. 2699–2711.
[13] Cereda, M., Xin, Y., Hamedani, H., Bellani, G., Kadlecek, S., Clapp, J., Guerra, L., 2017, "Tidal Changes on CT and Progression of ARDS," Thorax, **72**(11), pp. 981–989.
[14] Hamlington, K. L., Bates, J. H. T., Roy, G. S., Julianelle, A. J., Charlebois, C., Suki, B., and Smith, B. J., 2018, "Alveolar Leak Develops by a Rich-Get-Richer Process in Ventilator-Induced Lung Injury," PloS One, **13**(3), p. e0193934.
[15] Gaver, D. P., 3rd, Nieman, G. F., Gatto, L. A., Cereda, M., Habashi, N. M., and Bates, J. H. T., 2020, "The POOR Get POORer: A Hypothesis for the Pathogenesis of Ventilator-Induced Lung Injury," Am. J. Respir. Crit. Care Med., **202**(8), pp. 1081–1087.
[16] Curley, G. F., Laffey, J. G., Zhang, H., and Slutsky, A. S., 2016, "Biotrauma and Ventilator-Induced Lung Injury: Clinical Implications," Chest, **150**(5), pp. 1109–1117.
[17] Marini, J. J., and Gattinoni, L., 2020, "Time Course of Evolving Ventilator-Induced Lung Injury: The "Shrinking Baby Lung," Crit. Care Med., **48**(8), pp. 1203–1209.

[18] Acute Respiratory Distress Syndrome Network, 2000, "Ventilation With Lower Tidal Volumes as Compared With Traditional Tidal Volumes for Acute Lung Injury and the Acute Respiratory Distress Syndrome," N. Engl. J. Med., **342**(18), pp. 1301–1308.

[19] Amato, M. B., Meade, M. O., Slutsky, A. S., Brochard, L., Costa, E. L., Schoenfeld, D. A., Stewart, T. E., 2015, "Driving Pressure and Survival in the Acute Respiratory Distress Syndrome," N. Engl. J. Med., **372**(8), pp. 747–755.

[20] Kaczka, D. W., 2021, "Oscillatory Ventilation Redux: Alternative Perspectives on Ventilator-Induced Lung Injury in the Acute Respiratory Distress Syndrome," Curr. Opin. Physiol., **21**, pp. 36–43.

[21] Huhle, R., Pelosi, P., and de Abreu, M. G., 2016, "Variable Ventilation From Bench to Bedside," Crit. Care, **20**(1), p. 62.

[22] Jain, S. V., Kollisch-Singule, M., Sadowitz, B., Dombert, L., Satalin, J., Andrews, P., Gatto, L. A., Nieman, G. F., and Habashi, N. M., 2016, "The 30-Year Evolution of Airway Pressure Release Ventilation (APRV)," Intensive Care Med. Exp., **4**(1), p. 11.

[23] Guerin, C., Reignier, J., Richard, J. C., Beuret, P., Gacouin, A., Boulain, T., Mercier, E., 2013, "Prone Positioning in Severe Acute Respiratory Distress Syndrome," N. Engl. J. Med., **368**(23), pp. 2159–2168.

[24] Hess, D. R., 2015, "Recruitment Maneuvers and PEEP Titration," Respir. Care, **60**(11), pp. 1688–1704.

[25] Beitler, J. R., Sarge, T., Banner-Goodspeed, V. M., Gong, M. N., Cook, D., Novack, V., Loring, S. H., Talmor, D., and Group, E. P.-S., EPVent-2 Study Group, 2019, "Effect of Titrating Positive End-Expiratory Pressure (PEEP) With an Esophageal Pressure-Guided Strategy versus an Empirical High PEEP-FiO2 Strategy on Death and Days Free From Mechanical Ventilation Among Patients With Acute Respiratory Distress Syndrome: A Randomized Clinical Trial," JAMA, **321**(9), pp. 846–857.

[26] Abston, E., Herrmann, J., Taft, P., Eberlein, M., Kaczka, D. W., Stoltz, D. A., and Zabner, J., 2016, "The Effects of Chest Wall Strapping in a Porcine Model of ARDS," Am. J. Respir. Crit. Care Med., **193**, p. A4819.

[27] Marini, J. J., and Gattinoni, L., 2021, "Improving Lung Compliance by External Compression of the Chest Wall," Crit. Care, **25**(1), p. 264.

[28] Herrmann, J., Tawhai, M. H., and Kaczka, D. W., 2018, "Parenchymal Strain Heterogeneity During Oscillatory Ventilation: Why Two Frequencies Are Better Than One," J. Appl. Physiol. (1985), **124**(3), pp. 653–663.

[29] Herrmann, J., Tawhai, M. H., and Kaczka, D. W., 2019, "Computational Modeling of Primary Blast Lung Injury: Implications for Ventilator Management," Mil. Med., **184**(Suppl_1), pp. 273–281.

[30] Herrmann, J., Tawhai, M. H., and Kaczka, D. W., 2019, "Strain, Strain Rate, and Mechanical Power: An Optimization Comparison for Oscillatory Ventilation," Int. J. Numer. Method Biomed. Eng., **35**(10), p. e3238.

[31] Herrmann, J., Lilitwat, W., Tawhai, M. H., and Kaczka, D. W., 2020, "High-Frequency Oscillatory Ventilation and Ventilator-Induced Lung Injury: Size Does Matter," Crit. Care Med., **48**(1), pp. e66–e73.

[32] Bates, J. H. T., 2009, *Lung Mechanics: An Inverse Modeling Approach*, Cambridge University Press, Cambridge, UK.

[33] Kano, S., Lanteri, C. J., Duncan, A. W., and Sly, P. D., 1994, "Influence of Nonlinearities on Estimates of Respiratory Mechanics Using Multilinear Regression Analysis," J. Appl. Physiol., **77**(3), pp. 1185–1197.

[34] Ranieri, V. M., Zhang, H., Mascia, L., Aubin, M., Lin, C. Y., Mullen, J. B., Grasso, S., 2000, "Pressure-Time Curve Predicts Minimally Injurious Ventilatory Strategy in an Isolated Rat Lung Model," Anesthesiology, **93**(5), pp. 1320–132.

[35] Yuan, H., Suki, B., and Lutchen, K. R., 1998, "Sensitivity Analysis for Evaluating Nonlinear Models of Lung Mechanics," Ann. Biomed. Eng., **26**(2), pp. 230–241.

[36] Carvalho, A. R., Spieth, P. M., Pelosi, P., Vidal Melo, M. F., Koch, T., Jandre, F. C., Giannella-Neto, A., and Gama de Abreu, M., 2008, "Ability of Dynamic Airway Pressure Curve Profile and Elastance for Positive End-Expiratory Pressure Titration," Intensive Care Med., **34**(12), pp. 2291–2299.

[37] Kaczka, D. W., Barnas, G. M., Suki, B., and Lutchen, K. R., 1995, "Assessment of Time-Domain Analyses for Estimation of Low-Frequency Respiratory Mechanical Properties and Impedance Spectra," Ann. Biomed. Eng., **23**(2), pp. 135–151.

[38] King, G. G., Bates, J., Berger, K. I., Calverley, P., de Melo, P. L., Dellaca, R. L., Farre, R., 2020, "Technical Standards for Respiratory Oscillometry," Eur. Respir. J., **55**(2), p. 1900753.

[39] Kaczka, D. W., and Dellacà, R. L., 2011, "Oscillation Mechanics of the Respiratory System: Applications to Lung Disease," Crit. Rev. Biomed. Eng, **39**(4), pp. 337–359.

[40] Bates, J. H. T., Irvin, C. G., Farré, R., and Hantos, Z., 2011, "Oscillation Mechanics of the Respiratory System," Compr. Physiol., **1**(4), pp. 1233–1272.

[41] Otis, A. B., McKerrow, C. B., Bartlett, R. A., Mead, J., McIlroy, M. B., Selverstone, N. J., and Radford, E. P., 1956, "Mechanical Factors in Distribution of Pulmonary Ventilation," J. Appl. Physiol., **8**(4), pp. 427–443.

[42] Glapiński, J., Mroczka, J., and Polak, A. G., 2015, "Analysis of the Method for Ventilation Heterogeneity Assessment Using the Otis Model and Forced Oscillations," Comput. Methods Programs Biomed., **122**(3), pp. 330–340.

[43] Kaczka, D. W., Hager, D. N., Hawley, M. L., and Simon, B. A., 2005, "Quantifying Mechanical Heterogeneity in Canine Acute Lung Injury: Impact of Mean Airway Pressure," Anesthesiology, **103**(2), pp. 306–317.

[44] Suki, B., Yuan, H., Zhang, Q., and Lutchen, K. R., 1997, "Partitioning of Lung Tissue Response and Inhomogeneous Airway Constriction at the Airway Opening," J. Appl. Physiol., **82**(4), pp. 1349–1359.

[45] Kaczka, D. W., Brown, R. H., and Mitzner, W., 2009, "Assessment of Heterogeneous Airway Constriction in Dogs: A Structure-Function Analysis," J. Appl. Physiol., **106**(2), pp. 520–530.

[46] Kaczka, D. W., Mitzner, W., and Brown, R. H., 2013, "Effects of Lung Inflation on Airway Heterogeneity During Histaminergic Bronchoconstriction," J. Appl. Physiol., **115**(5), pp. 626–633.

[47] Kaczka, D. W., Massa, C. B., and Simon, B. A., 2007, "Reliability of Estimating Stochastic Lung Tissue Heterogeneity From Pulmonary Impedance Spectra: A Forward-Inverse Modeling Study," Ann. Biomed. Eng., **35**(10), pp. 1722–1738.

[48] Kaczka, D. W., Cao, K., Christensen, G. E., Bates, J. H. T., and Simon, B. A., 2011, "Analysis of Regional Mechanics in Canine Lung Injury Using Forced Oscillations and 3D Image Registration," Ann. Biomed. Eng., **39**(3), pp. 1112–1124.

[49] Akaike, H., 1974, "A New Look at the Statistical Model Identification," IEEE Trans. Automat. Control, **19**(6), pp. 716–723.

[50] Blanch, L., Romero, P. V., and Lucangelo, U., 2006, "Volumetric Capnography in the Mechanically Ventilated Patient," Minerva Anestesiol., **72**(6), pp. 577–585.

[51] Fletcher, R., Jonson, B., Cumming, G., and Brew, J., 1981, "The Concept of Deadspace With Special Reference to the Single Breath Test for Carbon Dioxide," Br. J. Anaesth., **53**(1), pp. 77–88.

[52] Fowler, W. S., 1948, "Lung Function Studies; the Respiratory Dead Space," Am. J. Physiol., **154**(3), pp. 405–416.

[53] Klocke, R. A., 2006, "Dead Space: Simplicity to Complexity," J. Appl. Physiol., **100**(1), pp. 1–2.

[54] Verscheure, S., Massion, P. B., Verschuren, F., Damas, P., and Magder, S., 2016, "Volumetric Capnography: Lessons From the Past and Current Clinical Applications," Crit. Care, **20**(1), p. 184.

[55] Romero, P. V., Lucangelo, U., Lopez Aguilar, J., Fernandez, R., and Blanch, L., 1997, "Physiologically Based Indices of Volumetric Capnography in Patients Receiving Mechanical Ventilation," Eur. Respir. J., **10**(6), pp. 1309–1315.

[56] Robinson, P. D., Latzin, P., Verbanck, S., Hall, G. L., Horsley, A., Gappa, M., Thamrin, C., 2013, "Consensus Statement for Inert Gas Washout Measurement Using Multiple- and Single-Breath Tests," Eur. Respir. J., **41**(3), pp. 507–522.

[57] Becklake, M. R., 1952, "A New Index of the Intrapulmonary Mixture of Inspired Air," Thorax, **7**(1), pp. 111–116.

[58] Fuchs, S. I., Eder, J., Ellemunter, H., and Gappa, M., 2009, "Lung Clearance Index: Normal Values, Repeatability, and Reproducibility in Healthy Children and Adolescents," Pediatr. Pulmonol., **44**(12), pp. 1180–1185.

[59] Verbanck, S., and Paiva, M., 1990, "Model Simulations of Gas Mixing and Ventilation Distribution in the Human Lung," J. Appl. Physiol. (1985), **69**(6), pp. 2269–2279.

[60] Lewis, S. M., Evans, J. W., and Jalowayski, A. A., 1978, "Continuous Distributions of Specific Ventilation Recovered From Inert Gas Washout," J. Appl. Physiol. Respir. Environ. Exerc. Physiol., **44**(3), pp. 416–423.

[61] Hlastala, M. P., 1984, "Multiple Inert Gas Elimination Technique," J. Appl. Physiol., **56**(1), pp. 1–7.

[62] Wagner, P. D., 2008, "The Multiple Inert Gas Elimination Technique (MIGET)," Intensive Care Med., **34**(6), pp. 994–1001.

[63] Wagner, P. D., 1981, "Estimation of Distributions of Ventilation/Perfusion Ratios," Ann. Biomed. Eng., **9**(5–6), pp. 543–556.

[64] Wagner, P. D., Saltzman, H. A., and West, J. B., 1974, "Measurement of Continuous Distributions of Ventilation-Perfusion Ratios: Theory," J. Appl. Physiol., **36**(5), pp. 588–599.

[65] Kollisch-Singule, M., Emr, B., Smith, B., Roy, S., Jain, S., Satalin, J., Snyder, K., 2014, "Mechanical Breath Profile of Airway Pressure Release Ventilation: The Effect on Alveolar Recruitment and Microstrain in Acute Lung Injury," JAMA Surg., **149**(11), pp. 1138–1145.

[66] Lehr, J. L., Butler, J. P., Westerman, P. A., Zatz, S. L., and Drazen, J. M., 1985, "Photographic Measurement of Pleural Surface Motion During Lung Oscillation," J. Appl. Physiol., **59**(2), pp. 623–633.

[67] Mariano, C. A., Sattari, S., Maghsoudi-Ganjeh, M., Tartibi, M., Lo, D. D., and Eskandari, M., 2020, "Novel Mechanical Strain Characterization of Ventilated Ex Vivo Porcine and Murine Lung Using Digital Image Correlation," Front. Physiol., **11**, p. 600492.

[68] Nieman, G. F., Bredenberg, C. E., Clark, W. R., and West, N. R., 1981, "Alveolar Function Following Surfactant Deactivation," J. Appl. Physiol. Respir. Environ. Exerc. Physiol., **51**(4), pp. 895–904.

[69] Namati, E., Thiesse, J., de Ryk, J., and McLennan, G., 2008, "Alveolar Dynamics During Respiration: Are the Pores of Kohn a Pathway to Recruitment?," Am. J. Respir. Cell Mol. Biol., **38**(5), pp. 572–578.

[70] Kollisch-Singule, M., Jain, S., Andrews, P., Smith, B. J., Hamlington-Smith, K. L., Roy, S., DiStefano, D., 2016, "Effect of Airway Pressure Release Ventilation on Dynamic Alveolar Heterogeneity," JAMA Surg., **151**(1), pp. 64–72.

[71] Mertens, M., Tabuchi, A., Meissner, S., Krueger, A., Schirrmann, K., Kertzscher, U., Pries, A. R., Slutsky, A. S., Koch, E., and Kuebler, W. M., 2009, "Alveolar Dynamics in Acute Lung Injury: Heterogeneous Distension Rather Than Cyclic Opening and Collapse," Crit. Care Med., **37**(9), pp. 2604–2611.

[72] Kollisch-Singule, M., Emr, B., Smith, B., Ruiz, C., Roy, S., Meng, Q., Jain, S., 2014, "Airway Pressure Release Ventilation Reduces Conducting Airway Micro-Strain in Lung Injury," J. Am. Coll. Surg., **219**(5), pp. 968–976.

[73] Fredberg, J. J., Keefe, D. H., Glass, G. M., Castile, R. G., and Frantz, I. D., 1984, "Alveolar Pressure Nonhomogeneity During Small-Amplitude High-Frequency Oscillation," J. Appl. Physiol., **57**(3), pp. 788–800.

[74] Davey, B. L. K., and Bates, J. H. T., 1993, "Regional Lung Impedance From Forced Oscillations Through Alveolar Capsules," Respir. Physiol., **91**(2–3), pp. 165–182.
[75] Mishima, M., Balassy, Z., and Bates, J. H. T., 1996, "Assessment of Local Lung Impedance by the Alveolar Capsule Oscillator in Dogs: A Model Analysis," J. Appl. Physiol., **80**(4), pp. 1165–1172.
[76] Fredberg, J. J., Ingram, R. H., Castile, R. G., Glass, G. M., and Drazen, J. M., 1985, "Nonhomogeneity of Lung Response to Inhaled Histamine Assessed With Alveolar Capsules," J. Appl. Physiol., **58**(6), pp. 1914–1922.
[77] Lauzon, A.-M., Dechman, G., and Bates, J. H. T., 1995, "On the Use of the Alveolar Capsule Technique to Study Bronchoconstriction," Respir. Physiol., **99**(1), pp. 139–146.
[78] Otis, D. R., Petak, F., Hantos, Z., Fredberg, J. J., and Kamm, R. D., 1996, "Airway Closure and Reopening Assessed by the Alveolar Capsule Oscillation Technique," J. Appl. Physiol., **80**(6), pp. 2077–2084.
[79] Cereda, M., Xin, Y., Goffi, A., Herrmann, J., Kaczka, D. W., Kavanagh, B. P., Perchiazzi, G., Yoshida, T., and Rizi, R. R., 2019, "Imaging the Injured Lung: Mechanisms of Action and Clinical Use," Anesthesiology, **131**(3), pp. 716–749.
[80] Simon, B. A., 2000, "Non-Invasive Imaging of Regional Lung Function Using x-Ray Computed Tomography," J. Clin. Monit. Comput., **16**(5/6), pp. 433–442.
[81] Lo, P., van Ginneken, B., Reinhardt, J. M., Yavarna, T., de Jong, P. A., Irving, B., Fetita, C., 2012, "Extraction of Airways From CT (EXACT'09)," IEEE Trans. Med. Imag., **31**(11), pp. 2093–2107.
[82] Van Rikxoort, E. M., and Van Ginneken, B., 2013, "Automated Segmentation of Pulmonary Structures in Thoracic Computed Tomography Scans: A Review," Phys. Med. Biol., **58**(17), pp. R187–R220.
[83] Gerard, S. E., Patton, T. J., Christensen, G. E., Bayouth, J. E., and Reinhardt, J. M., 2019, "FissureNet: A Deep Learning Approach for Pulmonary Fissure Detection in CT Images," IEEE Trans. Med. Imag., **38**(1), pp. 156–166.
[84] Gerard, S. E., Herrmann, J., Kaczka, D. W., Musch, G., Fernandez-Bustamante, A., and Reinhardt, J. M., 2020, "Multi-Resolution Convolutional Neural Networks for Fully Automated Segmentation of Acutely Injured Lungs in Multiple Species," Med. Image Anal., **60**, p. 101592.
[85] Simon, B. A., Kaczka, D. W., Bankier, A. A., and Parraga, G., 2012, "What Can Computed Tomography and Magnetic Resonance Imaging Tell us About Ventilation?," J. Appl. Physiol., **113**(4), pp. 647–657.
[86] Guerrero, T., Castillo, R., Sanders, K., Price, R., Komaki, R., and Cody, D., 2006, "Novel Method to Calculate Pulmonary Compliance Images in Rodents From Computed Tomography Acquired at Constant Pressures," Phys. Med. Biol., **51**(5), pp. 1101–1112.
[87] Christensen, G. E., Song, J. H., Lu, W., El Naqa, I., and Low, D. A., 2007, "Tracking Lung Tissue Motion and Expansion/Compression With Inverse Consistent Image Registration and Spirometry," Med. Phys., **34**(6Part1), pp. 2155–2163.
[88] Fardin, L., Broche, L., Lovric, G., Mittone, A., Stephanov, O., Larsson, A., Bravin, A., and Bayat, S., 2021, "Imaging Atelectrauma in Ventilator-Induced Lung Injury Using 4D x-Ray Microscopy," Sci. Rep., **11**(1), p. 4236.
[89] Yin, Y., Hoffman, E. A., Ding, K., Reinhardt, J. M., and Lin, C.-L., 2011, "A Cubic B-Spline-Based Hybrid Registration of Lung CT Images for a Dynamic Airway Geometric Model With Large Deformation," Phys. Med. Biol., **56**(1), pp. 203–218.
[90] Yin, Y., Hoffman, E. A., and Lin, C.-L., 2009, "Mass Preserving Nonrigid Registration of CT Lung Images Using Cubic B-Spline," Med. Phys., **36**(9Part1), pp. 4213–4222.
[91] Herrmann, J., Hoffman, E. A., and Kaczka, D. W., 2017, "Frequency-Selective Computed Tomography: Applications During Periodic Thoracic Motion," IEEE Trans. Med. Imag., **36**(8), pp. 1722–1732.
[92] Herrmann, J., Gerard, S. E., Shao, W., Xin, Y., Cereda, M., Reinhardt, J. M., Christensen, G. E., Hoffman, E. A., and Kaczka, D. W., 2021, "Effects of Lung Injury on Regional Aeration and Expiratory Time Constants: Insights From Four-Dimensional Computed Tomography Image Registration," Front. Physiol., **12**, p. 707119.
[93] Herrmann, J., Gerard, S. E., Shao, W., Hawley, M. L., Reinhardt, J. M., Christensen, G. E., Hoffman, E. A., and Kaczka, D. W., 2020, "Quantifying Regional Lung Deformation Using Four-Dimensional Computed Tomography: A Comparison of Conventional and Oscillatory Ventilation," Front. Physiol., **11**, p. 14.
[94] Alvarez, P., Rouze, S., Miga, M. I., Payan, Y., Dillenseger, J. L., and Chabanas, M., 2021, "A Hybrid, Image-Based and Biomechanics-Based Registration Approach to Markerless Intraoperative Nodule Localization During Video-Assisted Thoracoscopic Surgery," Med. Image Anal., **69**, p. 101983.
[95] Seyfi, B., Santhanam, A. P., and Ilegbusi, O. J., 2016, "A Biomechanical Model of Human Lung Deformation Utilizing Patient-Specific Elastic Property," J. Cancer Ther., **07**(06), pp. 402–415.
[96] Biederer, J., Beer, M., Hirsch, W., Wild, J. M., Fabel, M., Puderbach, M., and van Beek, E. J. R., 2012, "MRI of the Lung (2/3). Why… When … How?," Insights Imag., **3**(4), pp. 355–371.
[97] Biederer, J., Mirsadraee, S., Beer, M., Molinari, F., Hintze, C., Bauman, G., Both, M., van Beek, E. J. R., Wild, J. M., and Puderbach, M., 2012, "MRI of the Lung (3/3)-Current Applications and Future Perspectives," Insights Imag., **3**(4), pp. 373–386.
[98] Wild, J. M., Marshall, H., Bock, M., Schad, L. R., Jakob, P. M., Puderbach, M., Molinari, F., van Beek, E. J. R., and Biederer, J., 2012, "MRI of the Lung (1/3): Methods," Insights Imag., **3**(4), pp. 345–353.
[99] Fabel, M., Wintersperger, B. J., Dietrich, O., Eichinger, M., Fink, C., Puderbach, M., Kauczor, H.-U., Schoenberg, S. O., and Biederer, J., 2009, "MRI of Respiratory Dynamics With 2D Steady-State Free-Precession and 2D Gradient Echo Sequences at 1.5 and 3 Tesla: An Observer Preference Study," Eur. Radiol., **19**(2), pp. 391–399.
[100] Tetzlaff, R., Schwarz, T., Kauczor, H.-U., Meinzer, H.-P., Puderbach, M., and Eichinger, M., 2010, "Lung Function Measurement of Single Lungs by Lung Area Segmentation on 2D Dynamic MRI," Acad. Radiol., **17**(4), pp. 496–503.
[101] Fu, M., Zhao, B., Carignan, C., Shosted, R. K., Perry, J. L., Kuehn, D. P., Liang, Z.-P., and Sutton, B. P., 2015, "High-Resolution Dynamic Speech Imaging With Joint Low-Rank and Sparsity Constraints," Magn. Reson. Med., **73**(5), pp. 1820–1832.
[102] Deshmane, A., Gulani, V., Griswold, M. A., and Seiberlich, N., 2012, "Parallel MR Imaging," J. Magn. Reson. Imag., **36**(1), pp. 55–72.
[103] Geethanath, S., Reddy, R., Konar, A. S., Imam, S., Sundaresan, R., D R, R. B., and Venkatesan, R., 2013, "Compressed Sensing MRI: A Review," Crit. Rev. Biomed. Eng., **41**(3), pp. 183–204.
[104] Jaspan, O. N., Fleysher, R., and Lipton, M. L., 2015, "Compressed Sensing MRI: A Review of the Clinical Literature," Br. J. Radiol., **88**(1056), p. 20150487.
[105] Johnson, K. M., Fain, S. B., Schiebler, M. L., and Nagle, S., 2013, "Optimized 3D Ultrashort Echo Time Pulmonary MRI," Magn. Reson. Med., **70**(5), pp. 1241–1250.
[106] Mariappan, Y. K., Glaser, K. J., Hubmayr, R. D., Manduca, A., Ehman, R. L., and McGee, K. P., 2011, "MR Elastography of Human Lung Parenchyma: Technical Development, Theoretical Modeling and In Vivo Validation," J. Magn. Reson. Imag., **33**(6), pp. 1351–1361.
[107] Mariappan, Y. K., Glaser, K. J., Levin, D. L., Vassallo, R., Hubmayr, R. D., Mottram, C., Ehman, R. L., and McGee, K. P., 2014, "Estimation of the Absolute Shear Stiffness of Human Lung Parenchyma Using 1H Spin Echo, Echo Planar MR Elastography," J. Magn. Reson. Imag., **40**(5), pp. 1230–1237.
[108] Napadow, V. J., Mai, V., Bankier, A., Gilbert, R. J., Edelman, R., and Chen, Q., 2001, "Determination of Regional Pulmonary Parenchymal Strain During Normal Respiration Using Spin Inversion Tagged Magnetization MRI," J. Magn. Reson. Imag., **13**(3), pp. 467–474.
[109] Chung, Y. E., Hong, S. R., Lee, M.-J., Lee, M., and Lee, H.-J., 2014, "Krypton-Enhanced Ventilation CT With Dual Energy Technique: Experimental Study for Optimal Krypton Concentration," Exp. Lung Res., **40**(9), pp. 439–446.
[110] Fuld, M. K., Halaweish, A. F., Newell, J. D., Krauss, B., and Hoffman, E. A., 2013, "Optimization of Dual-Energy Xenon-Computed Tomography for Quantitative Assessment of Regional Pulmonary Ventilation," Invest. Radiol., **48**(9), pp. 629–637.
[111] Musch, G., Layfield, J. D. H., Harris, R. S., Melo, M. F. V., Winkler, T., Callahan, R. J., Fischman, A. J., and Venegas, J. G., 2002, "Topographical Distribution of Pulmonary Perfusion and Ventilation, Assessed by PET in Supine and Prone Humans," J. Appl. Physiol., **93**(5), pp. 1841–1851.
[112] Bajc, M., Neilly, B., Miniati, M., Mortensen, J., and Jonson, B., 2010, "Methodology for Ventilation/Perfusion SPECT," Semin. Nucl. Med., **40**(6), pp. 415–425.
[113] Herrmann, J., Gerard, S. E., Reinhardt, J. M., Hoffman, E. A., and Kaczka, D. W., 2021, "Regional Gas Transport During Conventional and Oscillatory Ventilation Assessed by Xenon-Enhanced Computed Tomography," Ann. Biomed. Eng., **49**(9), pp. 2377–2388.
[114] Farrow, C. E., Salome, C. M., Harris, B. E., Bailey, D. L., Bailey, E., Berend, N., Young, I. H., and King, G. G., 2012, "Airway Closure on Imaging Relates to Airway Hyperresponsiveness and Peripheral Airway Disease in Asthma," J. Appl. Physiol. (1985), **113**(6), pp. 958–966.
[115] Farrow, C. E., Salome, C. M., Harris, B. E., Bailey, D. L., Berend, N., and King, G. G., 2017, "Peripheral Ventilation Heterogeneity Determines the Extent of Bronchoconstriction in Asthma," J. Appl. Physiol. (1985), **123**(5), pp. 1188–1194.
[116] Grist, J. T., Chen, M., Collier, G. J., Raman, B., Abueid, G., McIntyre, A., and Matthews, V., et al., 2021, "Hyperpolarized (129)Xe MRI Abnormalities in Dyspneic Patients 3 Months After COVID-19 Pneumonia: Preliminary Results," Radiology, **301**(1), pp. E353–e360.
[117] Wang, Z., He, M., Bier, E., Rankine, L., Schrank, G., Rajagopal, S., Huang, Y. C., Kelsey, C., Womack, S., Mammarappallil, J., and Driehuys, B., 2018, "Hyperpolarized (129) Xe Gas Transfer MRI: The Transition From 1.5T to 3T," Magn. Reson. Med., **80**(6), pp. 2374–2383.
[118] Cereda, M., Xin, Y., Kadlecek, S., Hamedani, H., Rajaei, J., Clapp, J., and Rizi, R. R., 2014, "Hyperpolarized Gas Diffusion MRI for the Study of Atelectasis and Acute Respiratory Distress Syndrome," NMR Biomed, **27**(12), pp. 1468–1478.
[119] Johansen, T., Winkler, T., Kelly, V. J., Osorio-Valencia, J. S., Greenblatt, E. E., Harris, R. S., and Venegas, J. G., 2016, "A Method for Mapping Regional Oxygen and CO2 Transfer in the Lung," Respir. Physiol. Neurobiol., **222**, pp. 29–47.
[120] Bodenstein, M., David, M., and Markstaller, K., 2009, "Principles of Electrical Impedance Tomography and Its Clinical Application," Crit. Care Med., **37**(2), pp. 713–724.
[121] Costa, E. L. V., Lima, R. G., and Amato, M. B. P., 2009, "Electrical Impedance Tomography," Curr. Opin. Crit. Care, **15**(1), pp. 18–24.
[122] Frerichs, I., Amato, M. B. P., van Kaam, A. H., Tingay, D. G., Zhao, Z., Grychtol, B., Bodenstein, M., 2017, "Chest Electrical Impedance Tomography Examination, Data Analysis, Terminology, Clinical Use and Recommendations: Consensus Statement of the TRanslational EIT developmeNt stuDy Group," Thorax, **72**(1), pp. 83–93.

[123] Wolf, G. K., Grychtol, B., Frerichs, I., Zurakowski, D., and Arnold, J. H., 2010, "Regional Lung Volume Changes During High-Frequency Oscillatory Ventilation," Pediatr. Crit. Care Med., **11**(5), pp. 610–615.
[124] Calderón, A. P., 2006, "On an Inverse Boundary Value Problem," Comput. Appl. Math., **25**(2–3), pp. 133–138.
[125] Allers, A., and Santosa, F., 1991, "Stability and Resolution Analysis of a Linearized Problem in Electrical Impedance Tomography," Inverse Probl., **7**(4), pp. 515–533.
[126] Fan, W., and Wang, H., 2011, "An Image Reconstruction Algorithm Based on Preconditioned LSQR for 3D EIT," 2011 IEEE International Instrumentation and Measurement Technology Conference, Hangzhou, China, May 9–12, pp. 1–6.
[127] Goharian, M., Soleimani, M., Jegatheesan, A., Chin, K., and Moran, G. R., 2008, "A DSP Based Multi-Frequency 3D Electrical Impedance Tomography System," Ann. Biomed. Eng., **36**(9), pp. 1594–1603.
[128] Grychtol, B., Müller, B., and Adler, A., 2016, "3D EIT Image Reconstruction With GREIT," Physiol. Meas., **37**(6), pp. 785–800.
[129] Wagenaar, J., and Adler, A., 2016, "Electrical Impedance Tomography in 3D Using Two Electrode Planes: Characterization and Evaluation," Physiol. Meas., **37**(6), pp. 922–937.
[130] Nagpal, P., Guo, J., Shin, K. M., Lim, J. K., Kim, K. B., Comellas, A. P., Kaczka, D. W., Peterson, S., Lee, C. H., and Hoffman, E. A., 2021, "Quantitative CT Imaging and Advanced Visualization Methods: Potential Application in Novel Coronavirus Disease 2019 (COVID-19) Pneumonia," BJR Open, **3**(1), p. 20200043.
[131] Gerard, S. E., Herrmann, J., Xin, Y., Martin, K. T., Rezoagli, E., Ippolito, D., Bellani, G., Cereda, M., Guo, J., Hoffman, E. A., Kaczka, D. W., and Reinhardt, J. M., 2021, "CT Image Segmentation for Inflamed and Fibrotic Lungs Using a Multi-Resolution Convolutional Neural Network," Sci. Rep., **11**(1), p. 1455.
[132] Mondoñedo, J. R., McNeil, J. S., Herrmann, J., Simon, B. A., and Kaczka, D. W., 2018, "Targeted Versus Continuous Delivery of Volatile Anesthetics During Cholinergic Bronchoconstriction," ASME J. Eng. Sci. Med. Diagn. Ther., **1**(3), p. 031003.